Optically induced lattice dynamics probed with ultrafast x-ray diffraction

H. J. Lee,[1] J. Workman,[1] J. S. Wark,[2] R. D. Averitt,[1] A. J. Taylor,[1] J. Roberts,[1] Q. McCulloch,[1] D. E. Hof,[1] N. Hur,[3] S.-W. Cheong,[3] and D. J. Funk[1]

[1]*Los Alamos National Laboratory, Los Alamos, New Mexico 87545, USA*

[2]*Department of Physics, Clarendon Laboratory, University of Oxford, Parks Road, Oxford OX1 3PU, United Kingdom*

[3]*Department of Physics and Astronomy, Rutgers University, Piscataway, New Jersey 08854, USA*

(Received 24 January 2008; published 29 April 2008)

We have studied the picosecond lattice dynamics of optically pumped hexagonal $LuMnO_3$ by using ultrafast x-ray diffraction. The results show a shift and broadening of the diffraction curve due to the stimulated lattice expansion. To understand the transient response of the lattice, the measured time- and angle-resolved diffraction curves are compared to a theoretical calculation based on the dynamical diffraction theory of coherent phonon propagation modified for the hexagonal crystal structure of $LuMnO_3$. Our simulations reveal that a large coupling coefficient (c_{13}) between the *a-b* plane and the *c* axis is required to fit the data. Though we interpret the transient response within the framework of thermal coherent phonons, we do not exclude the possibility of strong nonthermal coupling of the electronic excitation to the atomic framework. We compare this result to our previous coherent phonon studies of $LuMnO_3$ in which we used optical pump-probe spectroscopy.

DOI: 10.1103/PhysRevB.77.132301 PACS number(s): 78.47.−p, 61.05.cp, 63.20.K−, 75.47.Lx

Since the development of laser-based ultrafast x-ray sources, there has been extensive work on femtosecond x-ray diffraction measurements.[1] The coupling of structurally sensitive x-rays with time-resolved pump-probe techniques allows the tracking of time-dependent structural changes in condensed matter. Recent research has been focused on the study of coherent acoustic phonons,[1,2] nonthermal melting,[3] and anharmonic acoustic wave propagation in semiconductors.[4]

Coherent phonons can be generated by an instantaneous thermal stress generated with an optical pulse that induces a periodic modulation of the optical properties of the solids due to the propagating strain pulse.[5] While coherent acoustic phonons of solids have been investigated using femtosecond x-ray diffraction, the main focus has been on semiconductors.

In this Brief Report, we present a study on the lattice dynamics of optically pumped single crystal $LuMnO_3$. The lattice dynamics in this hexagonal manganite is observed by using time-resolved optical pump and x-ray probe measurements in a symmetric Bragg geometry. We have measured the shift and broadening of diffraction curve due to coherent acoustic phonons in $LuMnO_3$. We also compare the experimental data with simulations of the x-ray diffraction from dynamical diffraction theory.

$LuMnO_3$, which has a hexagonal structure, is a multiferroic material with a ferroelectric phase transition at $T_C > 1000$ K and an antiferromagnetic transition near $T_N \sim 90$ K.[6,7] The coexistence of ferroelectric and magnetism in this system provides the possibility for electric-magnetic interactions and the potential for this material's use in spintronics applications. Previously, Lim *et al.*[8] have observed a coherent oscillation of acoustic phonons using time-resolved optical pump-probe spectroscopy of $LuMnO_3$. In this case, the coherent phonons were observed through the intensity variations of the transmission and/or reflectivity via a modulation of the dielectric function resulting from the propagating strain pulse. However, how the relationship between the generated coherent phonons and the thermoelastic properties of the crystal was not revealed. In the experiments reported here, we clarify the existence of the coherent phonons in the hexagonal manganite and directly reveal how they propagate into the crystal and how the magnitude of the strain pulse depends on a large elastic coupling between the *c* axis and the *a-b* plane by using laser generated ultrafast x-rays that are diffracted from the laser-excited lattice. The resulting diffraction patterns are interpreted within the coherent phonon propagation model of Thomsen *et al.*[5] to elucidate the material response.

The x-ray pulse is generated by using ~100 mJ of an 800 nm 100 fs laser pulse focused onto a moving Al wire, as shown in Fig. 1. Al $K\alpha$ x rays are collected by using a spherical quartz $(10\bar{1}0)$ crystal (radius of 150 mm) held in Bragg geometry and focused onto the $LuMnO_3$ single crystal. The pump pulse is spatially overlapped with x-ray pulse and temporally delayed by using automated translation stages. The diameter of the optically pumped region and the region probed by the focused x-ray pulse are 1 cm and

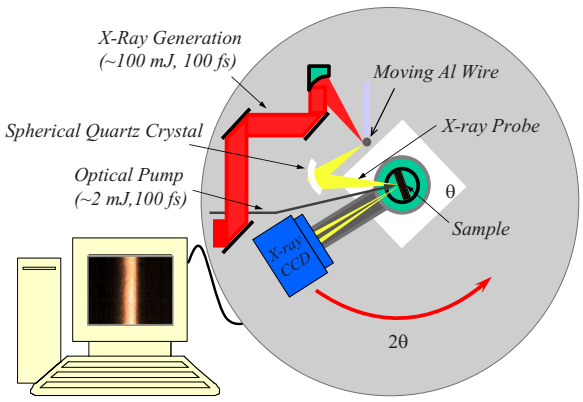

FIG. 1. (Color online) Schematic diagram of the ultrafast x-ray diffraction apparatus.

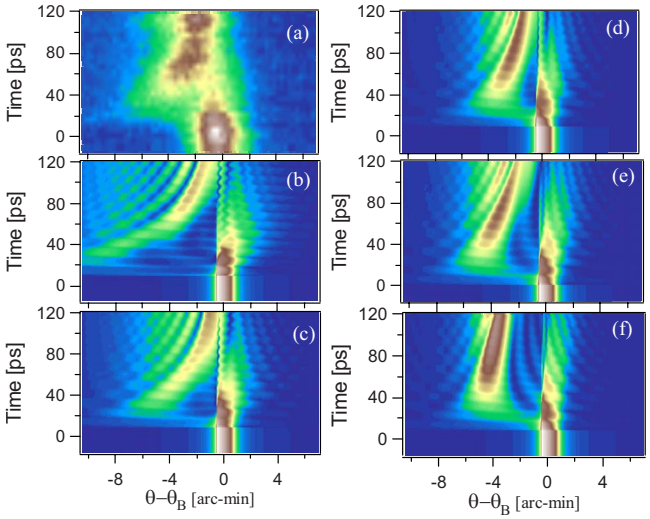

FIG. 2. (Color online) (a) Experimentally measured diffraction curve for $LuMnO_3$ with a laser fluence of 20 mJ/cm^2. Theoretically calculated diffraction curves with (b) $\zeta \sim 125$ nm and $c_{33}/c_{13} \sim 5.5 \pm 1$, (c) $\zeta \sim 125$ nm and $c_{33}/c_{13} \sim 11 \pm 1$, (d) $\zeta \sim 188$ nm and $c_{33}/c_{13} \sim 11 \pm 1$, (e) $\zeta \sim 250$ nm and $c_{33}/c_{13} \sim 5.5 \pm 1$, and (f) $\zeta \sim 250$ nm and $c_{33}/c_{13} \sim 5.5 \pm 1$.

600 μm, respectively. Detection is accomplished by using an x-ray sensitive charge-coupled device camera fixed at an angle for Bragg reflection from a (002) plane of $LuMnO_3$. Thus, time-resolved symmetric diffraction patterns are obtained from the laser-excited sample. The details of our experimental technique have been described previously.[9]

The optical penetration depth (ζ) of 800 nm light is ~ 125 nm for $LuMnO_3$.[10] This penetration depth allows the generation of large surface strains. We illuminate the crystal with laser pulse(s) having fluence(s) of $\sim 8-24$ mJ/cm^2. A significant fraction of the incident laser energy (pump pulse) is absorbed in the sample, causing a temperature jump in the absorbed volume (peak temperatures of 445 and 733 K for the 8 and 24 mJ/cm^2 cases, respectively, assuming a Debye temperature of 550 K). This rise in temperature generates the thermal stress that launches a bipolar strain wave that travels into the crystal, yielding the periodic modulation of the optical properties[8] and the changes in the location and broadening of the diffraction peak.

The experimentally measured and theoretically calculated time- and angle-resolved diffraction curves for $LuMnO_3$ are shown in Fig. 2. Figure 2(a) shows the shift of the position of the x-ray diffraction curve after excitation with ~ 20 mJ/cm^2 pump pulse. Here, we can see a very broad and low intensity diffraction curve in the negative Bragg angle region coexisting with the main curve immediately following photoexcitation. The shift and broadening are understood as the response of the lattice expansion due to the generation of the bipolar strain pulse. This deviated diffraction curve merges to the original diffraction line as delay time increases. Due to the anisotropic structure, $LuMnO_3$ has a strongly anisotropic thermal expansion when compared to a cubic system. While the equilibrium in-plane thermal expansion shows a thermal lattice expansion of 0.9% increase with temperature from 300 to 1000 K, the lattice expansion along the c axis shows just 0.1% increase with increasing temperature from 300 to 1000 K.[7] The natural elongation of the c axis of hexagonal manganite comes from the tilting of the MnO_5 polyhedron and the buckling of the rare earth plane. Therefore, the anisotropic thermal expansion is expected to give rise to a strong coupling between the elastic strain along the in-plane and c axis.

Many authors have discussed lattice expansion due to the effect of strain.[5,11,12] From dynamical diffraction theory, depth profiles of strain and the concomitant change in x-ray rocking curve have been accurately described. In particular, the propagation of the strain wave and the description of the lattice dynamics with acoustic coherent phonons have been proposed and compared to experimental data on semiconductors by Thomsen *et al.*[5] and Wie *et al.*[12] We have simulated our x-ray diffraction time dependence based on the equation written by Wie *et al.*,[12] using the bipolar strain description of Thomsen *et al.*[5] Because $LuMnO_3$ is a hexagonal crystal, the anisotropy must be accounted for in the thermoelastic behavior. To account for these physical differences, we have modified the bipolar strain equation to include the elasticity in the form

$$\sigma_3 = c_{33}\eta_3 - c_{33}\left(\frac{2c_{13}\beta_1}{c_{33}} + \beta_3\right)\Delta T,$$

where σ_3 is the elasticity in the z direction (normal to the surface, parallel to the c axis), c_{33} and c_{13} are components of the elastic strain tensors, β_1 and β_3 are the linear expansion coefficients in the x and z directions, and ΔT is a temperature rise. This results in changes to the bipolar strain equation,

$$\eta_3 = \left(\frac{2c_{13}\beta_1}{c_{33}} + \beta_3\right)\frac{Q(1-R)}{A\zeta C} \times \left\{e^{-z/\zeta}\left[1 - \frac{1}{2}e^{-|z-vt|/\zeta}\tanh\left(\frac{z-vt}{v\tau_{eph}}\right)\right]\right\},$$

where Q is the pulse energy, R is the reflectivity, A is the illuminated area, C is the specific heat, v is the sound velocity, and $\tau_{e\text{-}ph}$ is an electron-phonon coupling time.

Figures 2(b)–2(f) are theoretically calculated diffraction curves for $LuMnO_3$ from the above equations. By using known parameters for the specific heat,[6,13] linear expansion coefficients,[13] sound velocity,[8] penetration depth,[10] and density,[14] we numerically solved the equation. For penetration depth, we calculated an optical penetration depth ($\zeta \sim 125$ nm) from the optical constant obtained by Souchkov *et al.*[10] For c_{33}, we used the sound velocity from Lim *et al.*:[8] $\rho/c_{33} = v^2$. To calculate the diffraction, we varied only one unknown parameter, which is the elasticity tensor element c_{13}. Figures 2(b) and 2(c) show the simulation results with different c_{33}/c_{13} ratios ($\sim 5.5 \pm 1$ and $\sim 11 \pm 1$, respectively). Although Fig. 2(c) seems similar with the experimental result of Fig. 2(a), we varied ζ, in addition to the change in c_{33}/c_{13} ratio to find a best fit. Figures 2(d)–2(f) are obtained by using the different combinations of ζ and c_{33}/c_{13} values. To narrow the parameter space, we performed simulations with a larger skin depth (ζ) and a reasonable c_{33}/c_{13}

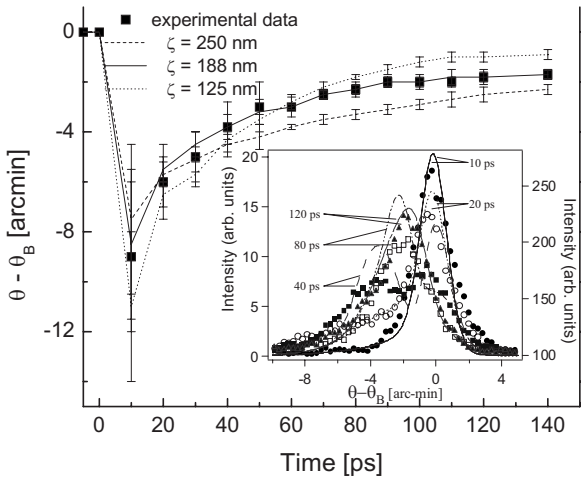

FIG. 3. Time dependent peak position of the shifted curves. Solid squares with error bars present shifted angles from the experimental result of Fig. 2(a). Dotted, solid, and dashed lines show shifted angles obtained from Figs. 2(c)–2(e) with error bars. The inset shows profile curves at each time delay. Symbols denote experimental results and lines are obtained from convolved Fig. 2(d).

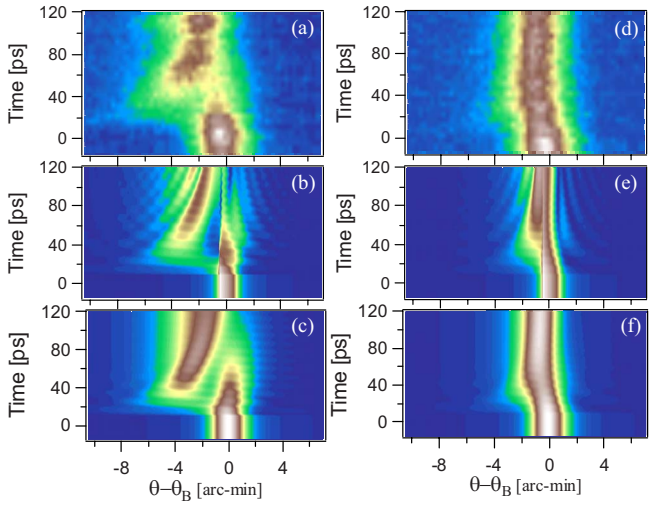

FIG. 4. (Color online) Experimental time- and angle-resolved diffractions of x rays from the (002) plane of $LuMnO_3$ with laser fluences of (a) 20 mJ/cm^2 and (d) 8 mJ/cm^2. (b) and (e) are theoretically calculated time- and angle-resolved diffraction curves with laser fluences of 20 and 8 mJ/cm^2 under $\zeta \sim 188$ nm and $c_{33}/c_{13} \sim 11 \pm 1$ parameter. (c) and (f) present convolved results with the Gaussian function from (b) and (e).

parametric ratio.[4] From the parametric study, we can see that Figs. 2(c)–2(e) are close to the experimental result of Fig. 2(a).

To further correlate the experimental and the simulation curves, we compared the peak position of the shifted diffraction curves of both the experimental and simulation results at selected time delays. The solid squares of Fig. 3 show the peak positions of the shifted curve of Fig. 2(a) at each time delay. We obtained peak positions from convolved curves of Fig. 2(c) (dotted line), Fig. 2(d) (solid line), and Fig. 2(e) (dashed line), as shown in Fig. 3. Although the three lineouts show good agreement with experimental data (they lie within the error bars at early times), the best agreement throughout the temporal range of the experiment is found for the calculation that used $\zeta \sim 188$ nm. The inset of Fig. 3 presents profiles of the experimental curve and convolved Fig. 2(d) at selected time delays. Profiles at 0, 20, and 120 ps show very good agreement between the experiment and the simulations. At 40 and 80 ps, the peak position of the experiment and the simulation agree well, but there exist differences in intensity in both the shifted and initial diffractions.[15]

Thus, there appears to be a discrepancy between our best-fit simulation of the experimental data, which yields 188 nm for the optical penetration depth, and the measured skin depth of 125 nm. This could result from our neglecting two-photon absorption, excited-state absorption, and ambipolar diffusion. Alternatively, the 188 nm value could simply result from rapid carrier diffusion, indicating that the strain is produced over a region larger than the optical penetration depth.[4] In either case, the strain field appears to be on a length scale approximately 50% greater than the skin depth. After fixing the unknown parameter ($c_{33}/c_{13} \sim 11 \pm 1$) and penetration depth ($\zeta \sim 188$ nm), we simulated it as a function of pump laser intensity to compare it with our available experimental results. Figures 4(a) and 4(d) are experimental results with pump fluences of 20 and 8 mJ/cm^2. We convolve Figs. 4(b) and 4(e) with a Gaussian instrument response function to yield Figs. 4(c) and 4(f). In Figs. 4(b) and 4(e), we can see the oscillatory signal resulted from the coherent acoustic phonon because the simulation has a "perfect" resolution. However, the oscillatory behavior is not observed in the experimental data due to noise and the instrument response function of our setup. Both calculations [Figs. 4(c) and 4(f)] are consistent with our experimental results.[16] At the longest time delay (which is not shown in this Brief Report), the diffraction peak slowly recovers due to the relaxed, but heated, lattice. At 600 ps, the recovery is still in progress. From the shifted peak position changes to 600 ps, we estimate an acoustic relaxation time of ~60 ps, which is approximately the mechanical relaxation time of the stressed layer within the penetration depth of the x rays.[1,17]

We have interpreted the data as resulting from a propagating strain pulse originating near the surface occurs by means of acoustic phonon generation and relaxation. While the optical study using two-color femtosecond optical pump-probe spectroscopy reported coherent acoustic phonons in the hexagonal manganite $LuMnO_3$, the x-ray diffraction results of Figs. 3(a) and 3(b) directly shows the propagation of the bipolar strain pulse generated by the lattice expansion and provides the data indicating that the structural coupling between the in-plane and c axis plays an important role within this interpretation. However, though we have analyzed the observed diffraction in terms of a coherent phonon model based on the thermal relaxation of the excited $LuMnO_3$, it is possible that the coherent excitation is the result of a direct excitation of the lattice structure through relaxation of the d-d excitation of $LuMnO_3$. The experiments discussed here cannot rule this out and we are considering other experiments (e.g., Raman, to observe Stokes–anti-Stokes ratio differences) to conclusively elucidate the mechanism.

In summary, we have observed the picosecond lattice dynamics of optically pumped $LuMnO_3$ by using ultrafast x-ray diffraction. A shift and broadening of the diffraction curve due to the stimulated lattice expansion has been compared to a theoretical calculation based on a dynamical diffraction theory. Within this framework, the calculation shows that the coupling between the in-plane and c axis plays an important role for propagating strain pulse in the hexagonal structure system. Further experiments on a material with negative thermal expansion (e.g., $YMnO_3$) and/or other techniques (e.g., Raman) will provide additional details that will permit us to understand the structural mechanistic dynamics of these manganites under thermal stress.

We thank J. S. Lee and M. F. DeCamp for helpful discussions. This work was performed, in part, at the Center for Integrated Nanotechnologies, a U.S. Department of Energy, Office of Basic Energy Sciences Nanoscale Science Research Center operated jointly by Los Alamos and Sandia National Laboratories. Los Alamos National Laboratory is a multiprogram laboratory operated by the University of California for the U.S. Department of Energy under Contract No. DE-AC52-06NA25396.

[1] C. Rose-Petruck, R. Jimenez, T. Guo, A. Cavalleri, C. W. Siders, F. Raksi, J. A. Squier, B. C. Walker, K. R. Wilson, and C. P. J. Barty, Nature (London) **398**, 310 (1999).

[2] A. M. Lindenberg, I. Kang, S. L. Johnson, T. Missalla, P. A. Heimann, Z. Chang, J. Larsson, P. H. Bucksbaum, H. C. Kapteyn, H. A. Padmore, R. W. Lee, J. S. Wark, and R. W. Falcone, Phys. Rev. Lett. **84**, 111 (2000).

[3] C. W. Siders, A. Cavalleri, K. Sokolowskitinten, C. Toth, T. Guo, M. Kammler, M. H. Vonhoegen, K. R. Wilson, D. Vonderlinde, and C. P. J. Barty, Science **286**, 1340 (1999).

[4] A. Cavalleri, C. W. Siders, F. L. H. Brown, D. M. Leitner, C. Tóth, J. A. Squier, C. P. J. Barty, K. R. Wilson, K. Sokolowski-Tinten, M. von der Linde, M. Kammler, and M. Horn von Hoegen, Phys. Rev. Lett. **85**, 586 (2000).

[5] C. Thomsen, H. T. Grahn, H. J. Maris, and J. Tauc, Phys. Rev. B **34**, 4129 (1986), and references therein.

[6] D. G. Tomuta, S. Ramakrishnan, G. J. Nieuwenhuys, and J. A. Mydosh, J. Phys.: Condens. Matter **13**, 4543 (2001).

[7] T. Katsufuji, M. Masaki, A. Machida, M. Moritomo, K. Kato, E. Nishibori, M. Takata, M. Sakata, K. Ohoyama, K. Kitazawa, and H. Takagi, Phys. Rev. B **66**, 134434 (2002).

[8] D. Lim, R. D. Averitt, J. Demsar, A. J. Taylor, N. Hur, and S.-W. Cheong, Appl. Phys. Lett. **83**, 4800 (2003).

[9] D. J. Funk, C. A. Meserole, D. E. Hof, G. L. Fisher, J. Roberts, A. J. Taylor, H. J. Lee, J. Workman, and Q. McCulloch, *Shock Compression of Condensed Matter* (AIP, Melville, NY, 2004), p. 1155.

[10] A. B. Souchkov, J. R. Simpson, M. Quijada, H. Ishibashi, N. Hur, J. S. Ahn, S. W. Cheong, A. J. Millis, and H. D. Drew, Phys. Rev. Lett. **91**, 027203 (2003).

[11] S. Takagi, Acta Crystallogr. **15**, 1311 (1962); D. Taupin, Bull. Soc. Fr. Mineral. Cristallogr. **87**, 469 (1964).

[12] C. R. Wie, T. A. Tombrello, and T. Vreeland, Jr., J. Appl. Phys. **59**, 3743 (1986).

[13] T. Katsufuji, S. Mori, M. Masaki, Y. Moritomo, N. Yamamoto, and H. Takagi, Phys. Rev. B **64**, 104419 (2001).

[14] We used a value of density calculated from the volume of one unit cell.

[15] We also compared the profiles of convolved Fig. 2(c) with profiles of the experimental curve, which is not shown in this Brief Report. The profiles of convolved Fig. 2(c) showed good agreement only at early time delay, but above 60 ps, it quickly recovered as compared to those of the experimental data.

[16] With a laser fluence of 8 mJ/cm^2, we also checked parameter combinations of ζ and c_{33}/c_{13}. While the calculation with $\zeta \sim 125$ nm shows a larger angle change than the experimental result and a quick recovery, the calculation with $\zeta \sim 250$ nm shows a similar angle shift with the experimental result and Fig. 4(f).

[17] From the sound velocity (7640 m/s) and the x-ray penetration depth (δ_x, 0.5 μm) at 1.48 keV, we can calculate a time from δ_x/ν, which approximates the mechanical relaxation time.